PCCP

ROYAL SOCIETY OF CHEMISTRY

PAPER

View Article Online
View Journal

Cite this: DOI: 10.1039/d6cp00779a

Electronic and structural properties of V_2O_5 layered polymorphs

Sakthi Kasthurirengan* and Hartwin Peelaers

V_2O_5 is a promising battery electrode material that can intercalate not only Li, but also more abundant alkaline metals such as Na and K, and even multivalent ions such as Al, Ca, Cu, Mg, and Zn. V_2O_5 exhibits several different polymorphs, and phase transitions between the polymorphs can occur depending on intercalant or external conditions. At least 8 different layered polymorphs have been observed. However, detailed information about the energetics and structural properties of each polymorph is still lacking. To obtain a reliable computational reference, we use hybrid density functional theory calculations to investigate the properties of layered V_2O_5 polymorphs. We benchmarked several methods to include van der Waals interactions in combination with hybrid functionals, and found that the Grimme D3 method is most accurate. We obtain detailed information on the electronic properties and structures of the various unintercalated polymorphs and show that the main electronic effect of intercalants is a filling of the lowest conduction bands, as the intercalant contributions are well above the conduction-band minimum. Despite the structural differences between the unintercalated polymorphs, we find that they have very similar band gaps and band structures, with the exception of the high temperature and pressure phase β.

Received 2nd March 2026,
Accepted 20th May 2026

DOI: 10.1039/d6cp00779a

rsc.li/pccp

1 Introduction

Lithium-ion batteries have become a ubiquitous part of our increasingly technologically-dependent lives. However, the growing demand for such batteries puts a large strain on available resources for both Li and the cathode materials. The high cost, coupled with safety concerns, also prevents widespread grid-scale usage.

Vanadium pentoxide, V_2O_5, is a viable alternative candidate cathode material,[1] as vanadium is abundant in the earth's crust.[2,3] It can reliably intercalate different intercalants, including Li,[4,5] Na,[6–8] K,[6,9] Mg,[6,10–15] Zn,[13,16–22] and Al.[13] Supercapacitors,[23,24] gaseous sensor materials,[25,26] and light-rechargeable Li-ion batteries[27] have been demonstrated. There are several chemical and physical synthesis routes to obtain V_2O_5, including RF and DC sputtering,[28,29] pulsed laser deposition,[30,31] chemical vapor deposition,[32] atomic layer deposition,[33] electrodeposition,[34] thermal evaporation,[35,36] thermal oxidation,[37] and the sol–gel method,[38] making V_2O_5 an appealing option for future batteries. The various synthesis routes and the inclusion of different intercalants leads to a wide variety of structural polymorphs which complicates the understanding of V_2O_5 fundamental properties.

In ambient conditions V_2O_5 stabilizes in an orthorhombic crystal structure, α-V_2O_5, with space group *Pmmn*. α-V_2O_5 is composed of weakly bonded layers of VO_5 square pyramids as shown in Fig. 1(a). For high temperatures and pressures, the layered β polymorph (space group $P2_1/m$) is found[39,40]

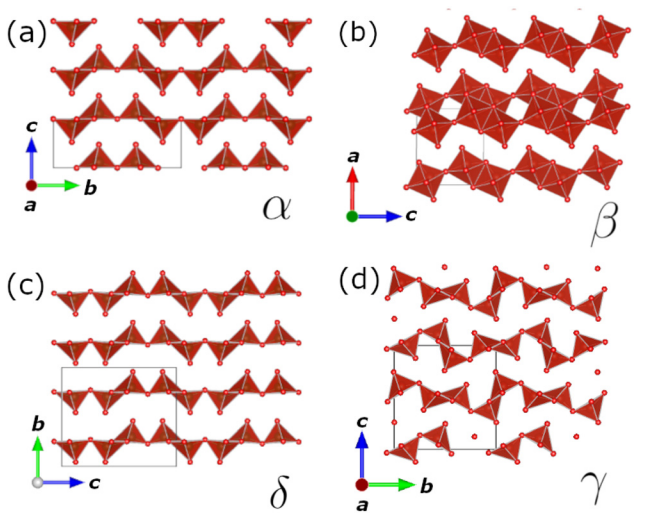

Fig. 1 The single-layer polymorphs investigated in this study: (a) α-V_2O_5, (b) β-V_2O_5, (c) δ-V_2O_5, and (d) γ-V_2O_5. Polyhedra are shown around the V atoms (large spheres) to indicate the bonding environment. Smaller spheres are O atoms.

Department of Physics and Astronomy, University of Kansas, Lawrence, KS 66045, USA. E-mail: skasthuri@ku.edu, peelaers@ku.edu

[Fig. 1(b)]. Upon Li intercalation ($Li_xV_2O_5$) several phase transitions take place.[1,41,42] The α-[Fig. 1(a)] and ε-structures maintain an orthorhombic (*Pmmn*) layered structure for concentration of $0 < x < 0.7$, with these phase transitions being reversible under delithiation.[42,43] The α polymorph is the ground state and is stable for $0 < x < 0.1$. The ε polymorph occurs for $0.35 < x < 0.7$. We were unable to stabilize this polymorph without the presence of Li, so it is not shown in Fig. 1. The δ polymorph [Fig. 1(c)] is observed for the range $0.7 < x < 1$ and has space group *Cmcm*.[42] This polymorph is similar to the α phase except that each alternate layer is shifted along the *b* axis or [010] plane by a distance of $b/2$.[41] It has also been observed when intercalating with Mg.[44,45]

For $1 < x < 2$, V_2O_5 occurs in the γ polymorph (*Pnma* space group) [Fig. 1(d)], which has been shown to be an irreversible transformation under delithiation.[46] Initial studies of this polymorph showed high energy densities.[4,47]

For $x > 2$, V_2O_5 occurs in the ω polymorph which is no longer layered as it has a rock-salt structure.[1] This structure was initially thought to be an irreversible transformation,[4] but delithiation of this polymorph leads to a disordered structure called β-$Li_{0.3}V_2O_5$.[5]

When V_2O_5 is intercalated with larger ions (compared to Li), so-called double-layer structures composed of distorted octahedra can be observed, as discussed in detail in ref. 41. Fig. 2 shows 3 different double-layer structures, which differ in how the octahedra are stacked in each layer. The shift in the [100] direction of each of the layers is characterized in units of Oc = 3.8 Å (the diagonal length across an octahedra).[41] The structure with a shift of 0 Oc is called the δ polymorph or D4 (following Galy's notation[41]) [see Fig. 2(a)], which is observed when intercalating with Ag.[48,49] When one layer of the D4 structure is shifted by +1 Oc, the ε polymorph [Fig. 2(b)] is obtained, observed with Cu intercalation.[49,50] The D4 structure with a −0.5 Oc shift is the ν polymorph [Fig. 2(c)], which occurs under Ca intercalation.[51] And finally, stacking alternate layers of D4 and D4M (the mirror image of the D4 structure) yields the ρ polymorph [Fig. 2(d)], which is observed with K intercalation.[52] The δ and ε labels for these double-layer polymorphs are not the same as, or even related to, the structures of the δ and ε single-layer polymorphs. To avoid confusion caused by this historical naming convention we will suffix the double-layer polymorphs by their first observed intercalants (as reported in ref. 41 and references therein).

While most of these polymorphs have been reported in intercalated forms, unintercalated polymorphs can be synthesized experimentally by topotactic removal of ions using strong oxidizing agents. For example, single layer polymorphs α and γ have been reported in a fully delithiated state.[53] β, which can accommodate sodium reversibly,[54] can be produced unintercalated at high pressure-high temperature conditions.[39,55] The bilayered ε-Cu phase formed with Cu in concentrations between 0.8–1, can be leached of all copper with an oxidizing treatment leaving the bilayered structure intact.[56]

Here, we explore the structural and energetic properties of the layered V_2O_5 polymorphs using first-principles calculations with hybrid functionals. We benchmark various methods of including van der Waals interactions in combination with hybrid functionals, finding that the Grimme D3 method performs best for this class of materials. We compare calculated structural parameters with experimentally reported values and analyze the (meta)stability of the polymorphs. We show that the electronic band structure of all layered polymorphs, despite the large structural differences, especially between single- and double-layered polymorphs, is remarkably similar. The magnitude of the band gap and the band characters of the valence and conduction bands are similar, and all exhibit a split-off conduction band (with the exception of the high temperature and pressure β phase). Finally, we briefly discuss the electronic effects of intercalants. We show that their energy levels are located high in the conduction bands, so that their main electronic contribution is the addition of electrons to the split-off bands. This in turn leads to a lowering of the filled, or half-filled, conduction bands. Combined, these results form a systematic computational reference of layered V_2O_5 polymorphs.

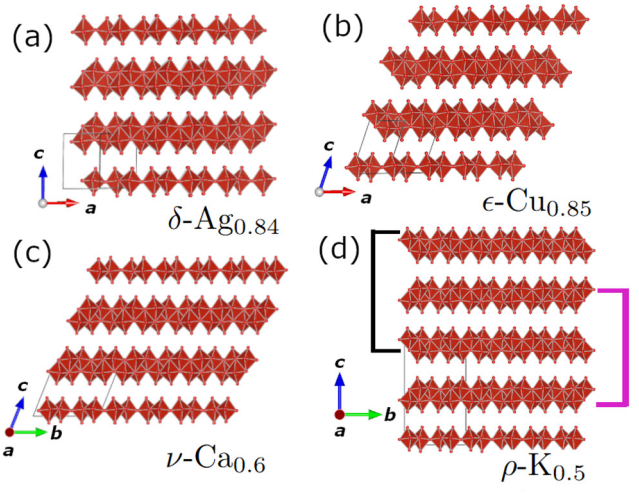

Fig. 2 The double-layer polymorphs investigated in this study: (a) δ-$Ag_{0.84}$–V_2O_5, (b) ε-$Cu_{0.85}$–V_2O_5, (c) ν-$Ca_{0.6}$–V_2O_5, and (d) ρ-$K_{0.5}$–V_2O_5. The black and purple indicators in (d) show that each alternating layer is identical and consists of D4 for the black layers and D4M for the purple layers.

2 Computational methods

We use density functional theory (DFT) with projector augmented wave (PAW) potentials[57] as implemented in the Vienna *Ab-initio* Simulation Package (VASP).[58,59] To obtain accurate structural and electronic properties we use the HSE06 hybrid functional.[60,61] A plane wave cutoff of 500 eV was used. All structures were relaxed so that the forces were smaller than 10 meV $Å^{-3}$ and the stresses smaller than 0.6 meV $Å^{-3}$. We use a $6 \times 4 \times 2$ *k*-point grid for the α polymorph, and equivalent *k*-point densities for the other polymorphs. The high-symmetry paths used for band structure calculations were obtained using the AFLOW package.[62] The site-projected band structures were

plotted using the pymatgen python code.[63] Structures are visualized using the VESTA code.[64]

2.1 van der Waals interactions

Given the layered nature of the considered polymorphs, and the lack of van der Waals (vdW) interactions in standard DFT functionals, including the hybrid functional HSE06 used here, we benchmarked several methods to include vdW interactions. We restricted ourselves to methods implemented in the VASP code and only those that are compatible with HSE06.[65–69] In practice, that restricts us to methods that are based on an inclusion of a multipole expansion term to capture the vdW interactions.[70,71] We used two different polymorphs (α and β) as test cases. The results are shown in Fig. 3, where we compare the lattice constants to experimental data.[39,72] The same data in tabular format can be found in the SI as Table S1. Not including any vdW interaction leads to a large error (7–10%) in the out-of-plane lattice direction, clearly indicating the need for including the vdW interactions. With vdW interactions included, the out-of-plane lattice constants are described more accurately, independent of the used approach.[65–69,73] The in-plane lattice constants do not depend strongly on the specific approach to include vdW interactions. Overall, the Grimme D3[67] was the most accurate, hence we used this functional for all other calculations. We also tested the B polymorph, which is not layered (see Table S2 in SI), to confirm that the inclusion of vdW interactions does not lead to errors in non-layered polymorphs, such as overbinding.

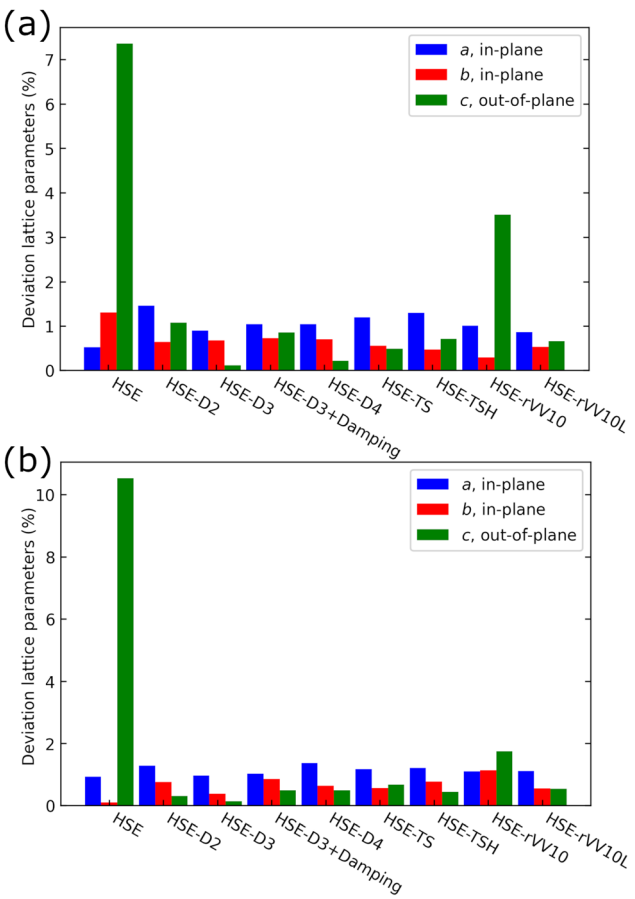

Fig. 3 Deviation (in percent) of the calculated lattice constants as compared to the experimental lattice constants,[39,72] for different computational methods[65–69] for the (a) α- and (b) β-V_2O_5 polymorphs.

3 Structural properties

We fully relaxed 8 layered unintercalated polymorphs (4 single-layer and 4 double-layer) and listed the lattice constants in Table 1. We compare with available experimental results.[39,41,43,44,46,47,72,74] Note that even for experimentally intercalated structures, we still obtain excellent agreement between our predictions and the observed lattice constants, which might indicate that the main role of the intercalants is the stabilization of the structure, while donating electrons to the conduction band. We will further validate this hypothesis in Section 5.

Energetically, we find that the α polymorph is indeed the ground state structure. The γ polymorph is 0.07 eV per formula unit (f.u.) higher in energy with a similar volume, while the other single-layer polymorphs are much higher in energy, 0.16 eV $f.u.^{-1}$ for β and 0.22 eV $f.u.^{-1}$ for δ, with large volume differences. The double-layered polymorphs are significantly higher in energy [at least 0.27 eV $f.u.^{-1}$ (for ε-$Cu_{0.85}$)], with ε-$Cu_{0.85}$ having a similar volume to the single-layer α polymorph, and the other double-layered polymorphs having increased volume. These energetics and volumes are reported in Fig. 4.

4 Electronic properties

Next, we turn our attention to the electronic structure of these polymorphs, where we focus on the single-layer α and the double-layer ε-$Cu_{0.85}$ polymorph. Band structures corresponding to the other layered polymorphs are provided in the SI.

Table 2 lists the calculated direct and indirect band gaps, the location of the valence-band maximum (VBM) and

Table 1 Calculated deintercalated lattice constants for the considered single-layer polymorphs (α, β, δ, and γ) and double-layer polymorphs (δ-$Ag_{0.84}$, ε-$Cu_{0.85}$, ν-$Ca_{0.6}$, and ρ-$K_{0.5}$) as compared to experimental values. The out-of-plane lattice directions are labeled with a star*

	a (Å)	*b* (Å)	*c* (Å)	*β* (deg.)	Space Group
α	11.43	3.53	4.36*	—	*Pmmn*
Exp. α[72]	11.51	3.56	4.37*	—	*Pmmn*
β	7.12*	3.53	6.26	90.39	$P2_1/m$
Exp. β[39]	7.11*	3.58	6.29	90.15	$P2_1/m$
δ	3.53	9.74*	11.31	—	*Cmcm*
Exp. δ[44]	3.70	9.97*	11.02	—	*Cmcm*
γ	9.88	3.56	10.05*	—	*Pnma*
Exp. γ[46,47]	9.95	3.59	10.04*	—	*Pnma*
δ-$Ag_{0.84}$	11.68	3.53	8.75*	91.03	*C2/m*
Exp. δ-$Ag_{0.84}$[74]	11.77	3.67	8.74*	90.54	*C2/m*
ε-$Cu_{0.85}$	11.5	3.58	9.01*	108.78	*C2/m*
Exp. ε-$Cu_{0.85}$[43]	11.7	3.63	8.84*	109.6	*C2/m*
ν-$Ca_{0.6}$	11.52	3.58	9.50*	111.65	*C2/m*
Exp. ν-$Ca_{0.6}$[41]	11.81	3.71	9.27*	101.9	*C2/m*
ρ-$K_{0.5}$	11.49	3.58	18.63*	—	*Cmcm*
Exp. ρ-$K_{0.5}$[41]	11.61	3.67	18.67*	—	*Ccmm*

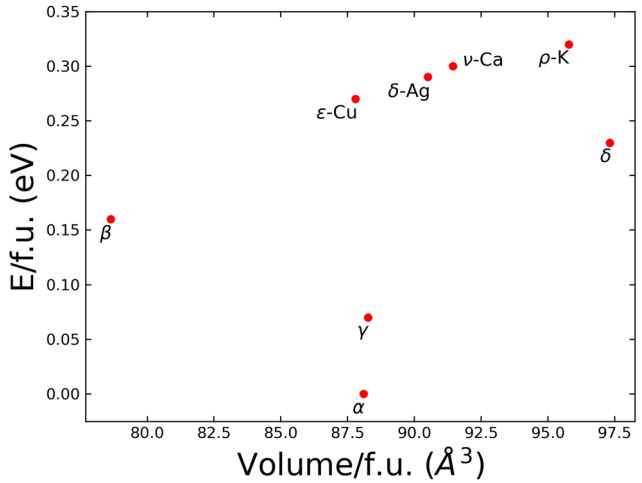

Fig. 4 The energy per formula unit (f.u.) as function of volume per formula unit for various layered V_2O_5 polymorphs. The energy per formula unit of the α polymorph is set to 0.

Table 2 Location of the VBM and CBM, magnitude of the indirect and direct band gap at the Γ point, and the energy separation of the split-off band. All energies are in eV

	VBM	CBM	$E_{gap}^{indirect}$	E_{gap}^{direct}	$E^{split-off}$
α	S → Y	Γ	3.18	3.78	0.61
β	C → E	Y	2.74	3.06	—
δ	A_1 → T	Γ	3.69	3.84	0.60
γ	Z → U	Γ	3.38	3.55	0.58
δ-$Ag_{0.84}$	I_1 → Z	Γ	3.47	3.8	0.6
ε-$Cu_{0.85}$	I_1 → Z	Z	3.37	3.8	0.57
ν-$Ca_{0.6}$	Γ → X	Γ	3.45	3.79	0.6
ρ-$K_{0.5}$	Γ → X	Γ	3.46	3.79	0.58

conduction-band minimum (CBM), and the separation between the split-off bands and the other conduction bands. In all considered polymorphs the band gap is found to be indirect, with the VBM occurring on different high-symmetry lines, as indicated in the table. For the ground state α polymorph we find an indirect gap of 3.18 eV and a direct gap of 3.78 eV. Experimentally, the direct optical band gap for the α polymorph was measured to be 2.35 eV.[75] Calculations at the quasiparticle self-consistent GW (QSGW) level obtain indirect band gaps of 3.8–4.0 eV and direct gaps at Γof 4.4–4.8 eV.[76–78] The discrepancy with the measured optical gap is attributed to excitons.[77,78] Our HSE06 results underestimate the fundamental band gaps by 0.7 eV. The mixing parameter has to be increased to 35% to obtain a better match. A test calculation for the double-layer ε-$Cu_{0.85}$ polymorph, at 35%, shows that the main effect of changing the mixing parameter is an increase of both the direct and indirect band gaps by 0.7 eV. Due to this systematic underestimation of the band gaps we opted to keep the default mixing parameter.

The resulting band structures of single- and double-layer polymorphs are remarkably similar, as illustrated in Fig. 5. The color scale corresponds to the orbital decomposition of the bands, where blue indicates O p character and red V d

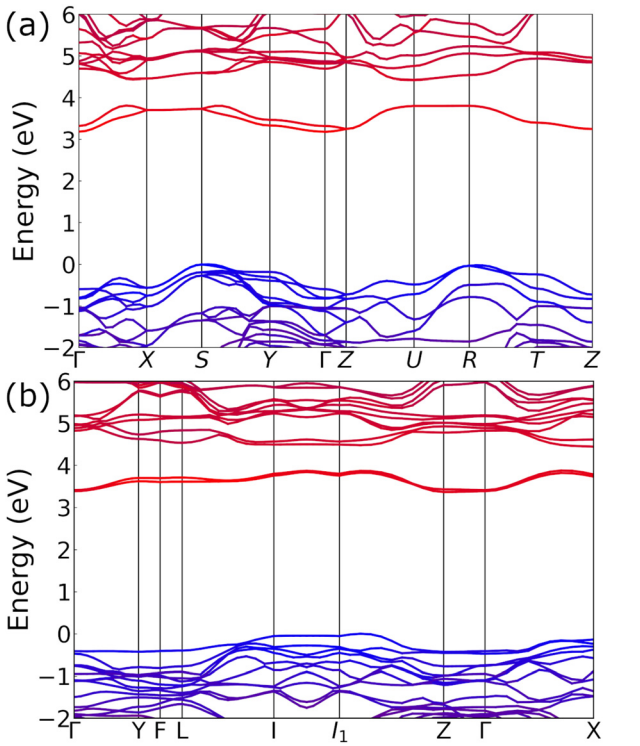

Fig. 5 The calculated band structures for the (a) single-layer α-V_2O_5 polymorph and (b) the double-layer ε-$Cu_{0.85}$ polymorph. The colors represent the band character, where red colors indicate V d character and blue O p character.

character. The highest valence bands are composed primarily of O 2p orbitals, while the lowest conduction bands are primarily V 3d. Orbital mixing occurs for lower valence or higher conduction bands. All polymorphs exhibit split-off bands that are ∼0.6 eV below the other conduction bands (see Table 2). The split-off bands originate from V-d orbitals that have no antibonding interaction with the bridge oxygens (which link chains of V_2O_5 into layers).[76] However, in the high-temperature and high-pressure β polymorph the split-off band merges with the other conduction bands on the high-symmetry Γ–Z line. Band structures corresponding to the other single- and double-layered polymorphs are shown in the SI (Fig. S1–S8). Due to the similar band characters for valence and conduction bands, all polymorphs have similar direct and indirect band gaps, with the exception of the high-temperature and high-pressure β polymorph. The electronic properties of all polymorphs are therefore extremely similar.

5 Electronic role of intercalants

Thus far, we focused on unintercalated polymorphs. We will consider the role of intercalants on the electronic properties next. The role of intercalants in the α-V_2O_5 polymorph was previously studied computationally for intercalation with Li,[79] Na,[76] and both Li and Mg.[80] Intercalation in the γ polymorph was studied for Li and Na.[81] Consistently, these works show that the intercalant orbitals do not lead to states within the

band gap region. The band gap region itself does contain bands with V-d character, but these correspond to lowered existing conduction band states.[79] These results are therefore consistent with our hypothesis that the primary electronic effect of intercalants is the formation of V-d character midgap states through the donation of electrons. Structurally, intercalants can stabilize phases, as evident from the experimental evidence detailed in the introduction, but here we are solely focusing on electronic properties.

We investigated the α single-layer and ε-$Cu_{0.85}$ bilayer polymorphs intercalated with 0.5 Li per formula unit. Information about more concentrations and other intercalants (Mg, Zn, K) can be found in the SI. For Na intercalation in α-V_2O_5 it was found that the magnetic moments on V-sites along the chain direction are antiferromagnetically (AFM) ordered.[76] We therefore explored both non-magnetic and AFM orderings in the α polymorph and found that for all concentrations and considered intercalants (Li^+, K^+, Mg^{2+}, and Zn^{2+}) that the AFM ordering is indeed the most favorable ordering (by ∼15 meV per formula unit for Li, Mg, and Zn, and by 40 meV for K). In contrast, unintercalated α prefers a non-magnetic ordering.

In Fig. 6, we show the band structures for $Li_{0.5}V_2O_5$ in both the single-layer α (with AFM) and double-layer ε-$Cu_{0.85}$ polymorphs. We color coded the band structures so that V contributions are depicted in dark grey, O contributions in light grey, and Li contributions in red. These band structures immediately reveal that Li contributions are located high in the conduction bands (more than 5 eV above the CBM). Similarly for $Mg_{0.5}$ (Fig. S13 and S14), $K_{0.5}$ (Fig. S15 and S16), and $Zn_{0.5}$ (Fig. S17 and S18), the intercalant only contributes high above the CBM. Note that since Zn also has d orbitals, some small Zn contributions show up in the valence bands and its conduction band contribution is lower compared to the other intercalants (but still 4 eV above the CBM). We tested increased intercalant concentrations (that maintain the layered structure, *e.g.*, Li_1 shown in Fig. S11). The increase in intercalant concentration results in more available electrons, so that more of the split-off bands become occupied. The number of newly occupied bands only depends on the introduced carrier concentration, *e.g.*, Li_1 (Fig. S11) leads to the same number of occupied bands as $Mg_{0.5}$ (Fig. S13). The shape of these newly filled bands does depend slightly on the intercalants and their concentration, due to small relaxation effects of the underlying V_2O_5 structure.

Since all intercalant states are located well above the CBM, the corresponding electrons will fill the lowest conduction-band states, *i.e.*, those of the split-off bands. Once electrons occupy conduction bands, their band energies decrease, leading to a separation from the other conduction bands. Note that the now filled bands are either completely filled (as is the case for the α polymorph) or multiple split-off bands are partially filled (for the ε-$Cu_{0.85}$ polymorph). As such, our results show that, for the studied layered polymorphs, the changes in electronic structure upon intercalation are similar, and will therefore not lead to capacity fade.

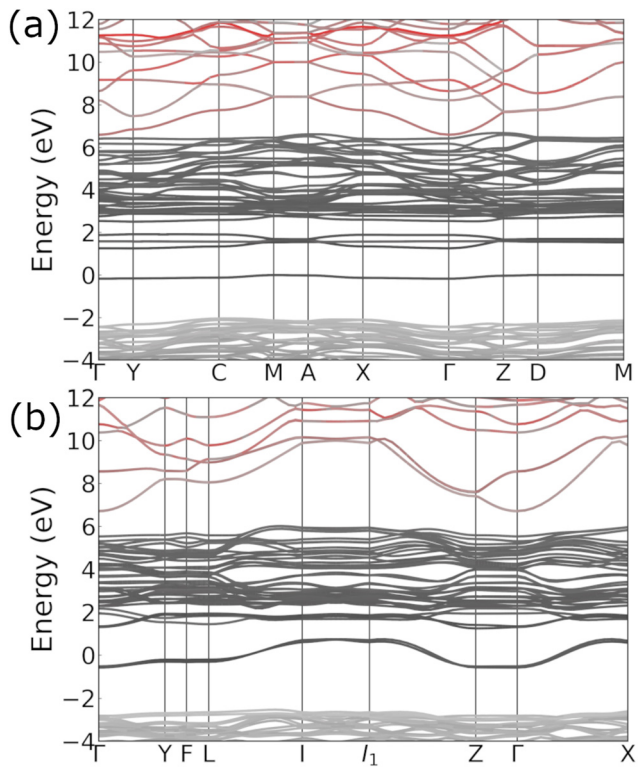

Fig. 6 The calculated band structures for a 0.5 Li per formula unit intercalation of the (a) single-layer α-V_2O_5 polymorph with AFM ordering and (b) the double-layer ε-$Cu_{0.85}$ polymorph. The V contribution is colored dark grey, the O contribution in light grey, and the Li contribution in red. The Fermi level is used as the energy 0 reference.

6 Conclusions

In conclusion, we performed a detailed first-principles study of 4 single-layer and 4 double-layer unintercalated V_2O_5 polymorphs using hybrid density functional theory. We compared several methods to include van der Waals interactions and found that the Grimme D3 method provided the most accurate results. Our band structure calculations reveal that independent of the studied polymorph, the band structure has very similar features: the topmost valence bands mainly consist of O p character, while the lowest conduction bands consist of V d orbitals. The lowest conduction bands are well separated from the other conduction bands, and the energy difference between these bands and the next conduction bands is around 0.6 eV for all polymorphs. The band gaps are also similar. Only the high-temperature and high-pressure β polymorph has a band structure where the split-off band merges with the other conduction bands for some of the high-symmetry directions, and a smaller band gap. We determined the main electronic role of intercalants for the α and ε-$Cu_{0.85}$ polymorphs. The contributions of Li^+, K^+, Mg^{2+}, and Zn^{2+} are located well above the conduction-band minimum. Their main role is therefore to donate electrons that will occupy the split-off bands, and upon occupation, lower the energy of these bands. Our results show that the electronic properties of various layered V_2O_5 polymorphs are

robust across all polymorphs, even when intercalants are present. This robustness will therefore also translate to V_2O_5-based cathodes upon cycling of batteries.

Conflicts of interest

There are no conflicts to declare.

Data availability

The data supporting this article have been included as part of the supplementary information (SI). Supplementary information: the SI contains tabular data (Tables S1 and S2) of lattice constants and percentage deviations from experiment of the single layer α, β, and nonlayered B polymorphs with respect to the various van der Waals interaction methods. Fig. S1–S8 show the electronic band structures of the unintercalated polymorphs. Fig. S9–S18 show the electronic band structures for the α and ε-$Cu_{0.85}$ polymorphs with Li, Mg, K and Zn intercalants. A zip file of our relaxed structures used for band structure calculations, in VASP POSCAR format, are also included. See DOI: https://doi.org/10.1039/d6cp00779a.

Acknowledgements

This work was supported by the National Science Foundation (NSF) through DMR-2339751 and by the University of Kansas General Research Fund allocation #2151089. This research used resources of the National Energy Research Scientific Computing Center, a DOE Office of Science User Facility supported by the Office of Science of the U.S. Department of Energy under Contract No. DE-AC02-05CH11231 using NERSC award BES-ERCAP0033524.

References

1 M. S. Whittingham, *Chem. Rev.*, 2004, **104**, 4271–4302.
2 G. J. Simandl and S. Paradis, *Appl. Earth Sci.*, 2022, **131**, 218–236.
3 B. Raja, *Steelworld*, 2007, **13**, 19–22.
4 C. Delmas, H. Cognac-Auradou, J. M. Cocciantelli, M. Ménétrier and J. P. Doumerc, *Solid State Ionics*, 1994, **69**, 257–264.
5 C. K. Christensen, D. R. Sørensen, J. Hvam and D. B. Ravnsbæk, *Chem. Mater.*, 2019, **31**, 512–520.
6 P. E. Tang, J. S. Sakamoto, E. Baudrin and B. Dunn, *J. Non-Cryst. Solids*, 2004, **350**, 67–72.
7 A. S. Etman, J. Sun and R. Younesi, *J. Energy Chem.*, 2019, **30**, 145–151.
8 N. Emery, R. Baddour-Hadjean, D. Batyrbekuly, B. Laïk, Z. Bakenov and J.-P. Pereira-Ramos, *Chem. Mater.*, 2018, **30**, 5305–5314.
9 M. Clites, J. L. Hart, M. L. Taheri and E. Pomerantseva, *ACS Energy Lett.*, 2018, **3**, 562–567.
10 R. Attias, M. Salama, B. Hirsch, Y. Gofer and D. Aurbach, *ChemElectroChem*, 2018, **5**, 3514–3524.
11 R. Attias, M. Salama, B. Hirsch, R. Pant, Y. Gofer and D. Aurbach, *ACS Energy Lett.*, 2019, **4**, 209–214.
12 F. Ming, H. Liang, Y. Lei, S. Kandambeth, M. Eddaoudi and H. N. Alshareef, *ACS Energy Lett.*, 2018, **3**, 2602–2609.
13 D. B. Le, S. Passerini, F. Coustier, J. Guo, T. Soderstrom, B. B. Owens and W. H. Smyrl, *Chem. Mater.*, 1998, **10**, 682–684.
14 G. Gershinsky, H. D. Yoo, Y. Gofer and D. Aurbach, *Langmuir*, 2013, **29**, 10964–10972.
15 R. Verrelli, A. P. Black, C. Pattanathummasid, D. S. Tchitchekova, A. Ponrouch, J. Oró-Solé, C. Frontera, F. Bardé, P. Rozier and M. R. Palacín, *J. Power Sources*, 2018, **407**, 162–172.
16 M. Yan, P. He, Y. Chen, S. Wang, Q. Wei, K. Zhao, X. Xu, Q. An, Y. Shuang, Y. Shao, K. T. Mueller, L. Mai, J. Liu and J. Yang, *Adv. Mater.*, 2018, **30**, 1703725.
17 P. Senguttuvan, S.-D. Han, S. Kim, A. L. Lipson, S. Tepavcevic, T. T. Fister, I. D. Bloom, A. K. Burrell and C. S. Johnson, *Adv. Energy Mater.*, 2016, **6**, 1600826.
18 N. Zhang, Y. Dong, M. Jia, X. Bian, Y. Wang, M. Qiu, J. Xu, Y. Liu, L. Jiao and F. Cheng, *ACS Energy Lett.*, 2018, **3**, 1366–1372.
19 X. Chen, L. Wang, H. Li, F. Cheng and J. Chen, *J. Energy Chem.*, 2019, **38**, 20–25.
20 A. Bhatia, J. Xu, J.-P. Pereira-Ramos, G. Rousse and R. Baddour-Hadjean, *Chem. Mater.*, 2022, **34**, 1203–1212.
21 Y. Hao, S. Zhang, P. Tao, T. Shen, Z. Huang, J. Yan and Y. Chen, *ChemNanoMat*, 2020, **6**, 797–805.
22 X. Guo, G. Fang, W. Zhang, J. Zhou, L. Shan, L. Wang, C. Wang, T. Lin, Y. Tang and S. Liang, *Adv. Energy Mater.*, 2018, **8**, 1801819.
23 P. M. Marley, G. A. Horrocks, K. E. Pelcher and S. Banerjee, *Chem. Commun.*, 2015, **51**, 5181–5198.
24 Z. Chen, V. Augustyn, J. Wen, Y. Zhang, M. Shen, B. Dunn and Y. Lu, *Adv. Mater.*, 2011, **23**, 791–795.
25 V. Modafferi, G. Panzera, A. Donato, P. L. Antonucci, C. Cannilla, N. Donato, D. Spadaro and G. Neri, *Sens. Actuators, B*, 2012, **163**, 61–68.
26 R. Suresh, K. Giribabu, R. Manigandan, S. P. Kumar, S. Munusamy, S. Muthamizh, A. Stephen and V. Narayanan, *Sens. Actuators, B*, 2014, **202**, 440–447.
27 B. D. Boruah, B. Wen and M. De Volder, *Nano Lett.*, 2021, **21**, 3527–3532.
28 L. Ottaviano, A. Pennisi, F. Simone and A. M. Salvi, *Opt. Mater.*, 2004, **27**, 307–313.
29 C. Navone, J. P. Pereira-Ramos, R. Baddour-Hadjean and R. Salot, *J. Power Sources*, 2005, **146**, 327–330.
30 C. Julien, E. Haro-Poniatowski, M. A. Camacho-López, L. Escobar-Alarcón and J. Jímenez-Jarquín, *Mater. Sci. Eng., B*, 1999, **65**, 170–176.
31 C. V. Ramana, R. J. Smith, O. M. Hussain, C. C. Chusuei and C. M. Julien, *Chem. Mater.*, 2005, **17**, 1213–1219.
32 C. Drosos, C. Jia, S. Mathew, R. G. Palgrave, B. Moss, A. Kafizas and D. Vernardou, *J. Power Sources*, 2018, **384**, 355–359.

33 X. Chen, E. Pomerantseva, P. Banerjee, K. Gregorczyk, R. Ghodssi and G. Rubloff, *Chem. Mater.*, 2012, **24**, 1255–1261.
34 J.-K. Lee, G.-P. Kim, I. K. Song and S.-H. Baeck, *Electrochem. Commun.*, 2009, **11**, 1571–1574.
35 R. Santos, J. Loureiro, A. Nogueira, E. Elangovan, J. V. Pinto, J. P. Veiga, T. Busani, E. Fortunato, R. Martins and I. Ferreira, *Appl. Surf. Sci.*, 2013, **282**, 590–594.
36 K.-C. Cheng, F.-R. Chen and J.-J. Kai, *Solar Energy Mater. Solar Cells*, 2006, **90**, 1156–1165.
37 J. S′wiatowska-Mrowiecka, V. Maurice, S. Zanna, L. Klein and P. Marcus, *Electrochim. Acta*, 2007, **52**, 5644–5653.
38 M. Gotic, S. Popovic, M. Ivanda and S. Music′, *Mater. Lett.*, 2003, **57**, 3186–3192.
39 P. Balog, D. Orosel, Z. Cancarevic, C. Schön and M. Jansen, *J. Alloys Compd.*, 2007, **429**, 87–98.
40 V. P. Filonenko and I. P. Zibrov, *Inorg. Mater.*, 2001, **37**, 7.
41 J. Galy, *J. Solid State Chem.*, 1992, **100**, 229–245.
42 R. Baddour-Hadjean, E. Raekelboom and J. P. Pereira-Ramos, *Chem. Mater.*, 2006, **18**, 3548–3556.
43 M. B. Smirnov, E. M. Roginskii, K. S. Smirnov, R. Baddour-Hadjean and J.-P. Pereira-Ramos, *Inorg. Chem.*, 2018, **57**, 9190–9204.
44 J.-C. Bouloux, I. Milosevic and J. Galy, *J. Solid State Chem.*, 1976, **16**, 393–398.
45 M. Onoda and A. Ohyama, *J. Phys.: Condens. Matter*, 1998, **10**, 1229.
46 J. M. Cocciantelli, M. Ménétrier, C. Delmas, J. P. Doumerc, M. Pouchard, M. Broussely and J. Labat, *Solid State Ionics*, 1995, **78**, 143–150.
47 R. Baddour-Hadjean, M. S. Renard and J. P. Pereira-Ramos, *J. Electrochem. Soc.*, 2019, **166**, A3474.
48 F. Garcia-Alvarado, J. M. Tarascon and B. Wilkens, *J. Electrochem. Soc.*, 1992, **139**, 3206.
49 J.-P. Monchoux, M. Dollé, P. Rozier and J. Galy, *Solid State Ionics*, 2011, **182**, 24–31.
50 J. Galy, D. Lavaud, A. Casalot and P. Hagenmuller, *J. Solid State Chem.*, 1970, **2**, 531–543.
51 A. Kutoglu, *Z. fur Krist.*, 1983, **162**, 263.
52 J.-M. Savariault and J. Galy, *J. Solid State Chem.*, 1992, **101**, 119–127.
53 R. Baddour-Hadjean, C. Navone and J. P. Pereira-Ramos, *Electrochim. Acta*, 2009, **54**, 6674–6679.
54 R. Córdoba, J. Goclon, A. Sarapulova, Q. Fu, J. Maibach, S. Dsoke, F. Fauth, A. Kuhn and F. García-Alvarado, *Appl. Res.*, 2023, **2**, e202200052.
55 R. Baddour-Hadjean, M. B. Smirnov, K. S. Smirnov, V. Y. Kazimirov, J. M. Gallardo-Amores, U. Amador, M. E. Arroyo-de Dompablo and J. P. Pereira-Ramos, *Inorg. Chem.*, 2012, **51**, 3194–3201.
56 R. Baddour-Hadjean, M. Safrany Renard, N. Emery, L. T. N. Huynh, M. L. P. Le and J. P. Pereira-Ramos, *Electrochim. Acta*, 2018, **270**, 129–137.
57 P. E. Blöchl, *Phys. Rev. B:Condens. Matter Mater. Phys.*, 1994, **50**, 17953–17979.
58 G. Kresse and J. Hafner, *Phys. Rev. B:Condens. Matter Mater. Phys.*, 1993, **47**, 558.
59 G. Kresse and J. Furthmüller, *Phys. Rev. B:Condens. Matter Mater. Phys.*, 1996, **54**, 11169–11186.
60 J. Heyd, G. E. Scuseria and M. Ernzerhof, *J. Chem. Phys.*, 2003, **118**, 8207–8215.
61 J. Heyd, G. E. Scuseria and M. Ernzerhof, *J. Chem. Phys.*, 2006, **124**, 219906.
62 S. Curtarolo, W. Setyawan, S. Wang, J. Xue, K. Yang, R. H. Taylor, G. L. Hart, S. Sanvito, M. B. Nardelli, N. Mingo and O. Levy, *Comput. Mater. Sci.*, 2012, **58**, 227–235.
63 S. P. Ong, W. D. Richards, A. Jain, G. Hautier, M. Kocher, S. Cholia, D. Gunter, V. L. Chevrier, K. A. Persson and G. Ceder, *Comput. Mater. Sci.*, 2013, **68**, 314–319.
64 K. Momma and F. Izumi, *J. Appl. Crystallogr.*, 2011, **44**, 1272–1276.
65 S. Grimme, *J. Comput. Chem.*, 2006, **27**, 1787–1799.
66 S. Grimme, J. Antony, S. Ehrlich and H. Krieg, *J. Chem. Phys.*, 2010, **132**, 154104.
67 S. Grimme, S. Ehrlich and L. Goerigk, *J. Comput. Chem.*, 2011, **32**, 1456–1465.
68 A. Tkatchenko and M. Scheffler, *Phys. Rev. Lett.*, 2009, **102**, 073005.
69 T. Bucko, S. Lebègue, J. G. Ángyán and J. Hafner, *J. Chem. Phys.*, 2014, **141**, 034114.
70 T. Bucko, S. Lebègue, J. Hafner and J. G. Ángyán, *Phys. Rev. B:Condens. Matter Mater. Phys.*, 2013, **87**, 064110.
71 H. Peelaers and C. G. Van de Walle, *J. Phys.: Condens. Matter*, 2014, **26**, 305502.
72 R. Enjalbert and J. Galy, *Acta Crystallogr., Sect. C: Cryst. Struct. Commun.*, 1986, **42**, 1467–1469.
73 E. Caldeweyher, C. Bannwarth and S. Grimme, *J. Chem. Phys.*, 2017, **147**, 034112.
74 P. Rozier, M. Dollé and J. Galy, *J. Solid State Chem.*, 2009, **182**, 1481–1491.
75 N. Kenny, C. R. Kannewurf and D. H. Whitmore, *J. Phys. Chem. Solids*, 1966, **27**, 1237–1246.
76 C. Bhandari and W. R. L. Lambrecht, *Phys. Rev. B:Condens. Matter Mater. Phys.*, 2015, **92**, 125133.
77 V. Gorelov, L. Reining, M. Feneberg, R. Goldhahn, A. Schleife, W. R. L. Lambrecht and M. Gatti, *npj Comput. Mater.*, 2022, **8**, 94.
78 C. Garcia, S. K. Radha, S. Acharya and W. R. L. Lambrecht, *Phys, Rev, B*, 2024, **110**, 085102.
79 P. Watthaisong, S. Jungthawan, P. Hirunsit and S. Suthirakun, *RSC Adv.*, 2019, **9**, 19483–19494.
80 R. Xiao, J. Xie, T. Luo, L. Huang, Y. Zhou, D. Yu, C. Chen and Y. Liu, *J. Phys. Chem. C*, 2018, **122**, 1513–1521.
81 E. M. Roginskii, M. B. Smirnov, K. S. Smirnov, R. Baddour-Hadjean, J.-P. Pereira-Ramos, A. N. Smirnov and V. Y. Davydov, *J. Phys. Chem. C*, 2021, **125**, 5848–5858.